Acta Cryst. (1987). A43, 322-326

X-ray Diffraction by a Low-Angle Twist Boundary Perpendicular to Crystal Surface. II. Plane-Wave Image Profiles

BY D. M. VARDANYAN

Department of Physics, Yerevan State University, Mravyan str. 1, 375049 *Yerevan, Armenia, USSR*

AND H. M. PETROSYAN

Department of Physics, Yerevan Pedagogical Institute, Khandjyan str. 5, 375010 *Yerevan, Armenia, USSR*

(*Received* 12 *August* 1985; *accepted* 21 *October* 1986)

Abstract

The formulae for the structure factor of a dislocation superlattice, obtained in paper I, are analyzed in a variety of situations. The plane-wave image profiles of a twist boundary perpendicular to the crystal surface are plotted for various values of the satellite order l and (**hb**), where **h** is the diffraction vector and **b** is the Burgers vector. The kinematic profiles are in qualitative agreement with the superstructure factor of the dislocation superlattice. Because of extinction, the dynamical profiles appreciably differ from the kinematic ones. The X-ray channelling through the twist boundary is demonstrated.

1. Introduction

In the previous paper (Vardanyan & Petrosyan, 1987), hereafter referred to as I, two-wave X-ray diffraction by a pure low-angle twist boundary perpendicular to the crystal surface is considered in the case when the dislocation superlattice (SL) period is much less than the crystal extinction length. The directions of the diffraction maxima were found (I-19) and a formula for the superstructure factor was obtained (I-23). In the present study the analysis of these formulae is performed. The superstructure-factor value on a boundary plane, as well as its asymptotic behavior far from the boundary, is determined. The low-angle twist boundary plane-wave image profiles are plotted in the kinematic and dynamical approaches. Absorption is not taken into account. The symbols are the same as those in I.

2. Analysis of the general formula (I-23)

Taking into account (I-21) and (I-22), we consider only the case $l \geq n$ and $\mathbf{hb} > 0$, so the sign of n is determined by that of y.

On a boundary plane $Y = 0$ ($q = 1$), from (I-23) we obtain

$$M_{l,n} = 2(-i)^n (\pi l)^{-1} \sin(\pi n/2), \qquad (1)$$

where we have used the following ratios (Bateman & Erdelyi, 1953):

$$F(a, b; c; 1) = \frac{\Gamma(c)\Gamma(c-a-b)}{\Gamma(c-a)\Gamma(c-b)}$$

$$\Gamma(x)\Gamma(1-x) = \pi/\sin(\pi x).$$

For the particular values of l, from (1), we have

$$M_{l,n} = \begin{cases} \delta_{0n} & \text{at } l = 0 \qquad (2a) \\ 0 & \text{at } l = 2k \neq 0 \qquad (2b) \\ -2i(\pi l)^{-1} & \text{at } l = 2k-1, \qquad (2c) \end{cases}$$

where δ_{ij} is the Kronecker symbol.

The boundary plane is a SL of stacking faults with the phase shift πn. Equations (2) coincide with the analogous formulae obtained by Vardanyan & Manoukyan (1982, 1985). Far from the boundary, at $|Y| \to \infty$ ($q \to 0$), from (I-23) we obtain the following asymptotic formulae:

$$M_{l,n} = \begin{cases} (-i)^n \dfrac{\Gamma(l/2)}{\Gamma(n/2)\Gamma[(l-n)/2+1]} q^{(l-n)/4} \\ \quad \text{at } l > n \qquad (3a) \\ (-i)^l (1 - ql^2/4) \quad \text{at } l = n > 0 \qquad (3b) \\ (-i)^{l+1} \dfrac{\Gamma(l/2)\sin(\pi l/2)}{\pi^{1/2}\Gamma[(l+1)/2]} (q/4)^{l/2} \\ \quad \text{at } l = -n > 0. \qquad (3c) \end{cases}$$

Here we have used the approximation

$$F(a, b; c; q) \simeq 1 + (ab/c)q.$$

The formulae (3b) and (I-21) show that the value $l = n > 0$ corresponds to the principal maximum of the block $y > 0$ and the value $l = n < 0$ corresponds to that of the block $y < 0$. On the basis of (I-19), we find the angular distance between the principal maxima of the blocks:

$$\Delta\theta = 2s_l/h = n/z_0 h = b/z_0$$

0108-7673/87/030322-05$01.50

Table 1. *The magnitudes* $|M_{l,n}|_{max}$, *locations* Y_m *and half-widths* ΔY_m *of the superstructure maxima for a few values of satellite number* l *and* $n = \mathbf{hb}$

l, n	$\lvert M_{l,n}\rvert_{max}$	πY_m	$\pi\Delta Y_m$	l, n	$\lvert M_{l,n}\rvert_{max}$	πY_m	$\pi\Delta Y_m$
0, 2	1	0	0·693	1, 1	—	—	—
0, 4	1	0	0·347	1, 3	0·855	0·112	0·652
0, 6	1	0	0·231	1, 5	0·850	0·065	0·366
0, 8	1	0	0·173	1, 7	0·847	0·047	0·256
2, 2	—	—	—	3, 1	0·285	0·112	0·652
2, 4	0·770	0·277	0·743	3, 3	0·266	0·024	0·124
2, 6	0·750	0·173	0·433	3, 5	0·265	0·016	0·075
2, 8	0·744	0·128	0·318		0·725	0·402	0·810
4, 2	0·385	0·277	0·743	3, 7	0·264	0·100	0·051
4, 4	0·333	0·100	0·185		0·297	0·270	0·460
4, 6	0·327	0·065	0·120	5, 1	0·170	0·065	0·366
	0·696	0·510	0·388	5, 3	0·159	0·016	0·075
4, 8	0·324	0·050	0·087		0·435	0·402	0·810
	0·656	0·358	0·478	5, 5	0·160	0·008	0·043
6, 2	0·250	0·173	0·433		0·360	0·184	0·221
6, 4	0·218	0·065	0·120	5, 7	0·158	0·050	0·029
	0·464	0·510	0·338		0·349	0·124	0·143
6, 6	0·214	0·044	0·076		0·678	0·602	0·831
	0·374	0·255	0·236	7, 1	0·121	0·047	0·256
6, 8	0·212	0·032	0·054	7, 3	0·113	0·010	0·051
	0·357	0·184	0·158		0·297	0·270	0·460
	0·664	0·665	0·842	7, 5	0·113	0·005	0·029
8, 2	0·186	0·128	0·318		0·249	0·124	0·143
8, 4	0·162	0·050	0·087		0·484	0·602	0·831
	0·328	0·358	0·478	7, 7	0·112	0·005	0·023
8, 6	0·159	0·032	0·054		0·241	0·086	0·097
	0·268	0·184	0·158		0·382	0·327	0·241
	0·498	0·665	0·842				
8, 8	0·158	0·024	0·025				
	0·258	0·132	0·107				
	0·387	0·390	0·253				

in agreement with (I-1). There are $(|n|-1)$ satellites between two principal maxima. From the theorem on the number of Gauss hypergeometric function zeros (Runckel, 1971), the number N of $|M_{l,n}|$ maxima may be determined as

$$N=\begin{cases}\min\left([(l+1)/2],[(n+1)/2]\right) & \text{at } l\neq n>0\\ [(l-1)/2] & \text{at } l=n\\ 1 & \text{at } l=0\\ 0 & \text{at } l>0,\ n<0,\end{cases} \tag{4}$$

where $[x]$ is the largest integer $\leq x$.

If $l>0$ and $\mathbf{hb}>0$, then all the maxima lie on the semiplane $y>0$.

The magnitudes, locations and half-widths of the $|M_{l,n}|$ maxima for a few values of l and n are given in Table 1.

We note the following:

(a) the maxima form an increasing sequence;

(b) with increasing l the maxima decrease;

(c) for a given l the values of the maxima and their half-widths weakly depend on n (except for the furthest from the boundary maximum);

(d) with increasing n the maxima shift towards the boundary;

(e) the maxima are located on one side of the boundary, except for the case $l=0$;

(f) for large l and n the maxima separation decreases, and they may merge.

Consider the cases of l being 0, even and odd.

(1) $l=0$

In this case, from (I-19), we have $s_0=0$, which corresponds to the satellite located in the middle of two principal maxima. The superstructure factor is defined by (I-25a):

$$M_{0,n}=q^{|n|/4}=\exp(-\pi nY). \tag{5}$$

In the boundary plane, $Y=0$, $M_{0,n}=1$ since at $l=0$ n is an even number and the phase shift is a multiple of 2π. Far from the boundary $M_{0,n}$ decreases rapidly from both sides of the boundary (Fig. 1). At $n=0$ ($\mathbf{hb}=0$) we have $M_{0,0}=1$, corresponding to the reflection from an ideal crystal, *i.e.* in this case the boundary is invisible. The maximum half-width is equal to

$$\Delta Y=2\ln 2/\pi|n| \tag{6}$$

and decreases with increasing $|n|$.

(2) *Even* l

Since l and n are of the same parity we set $l=2k>0$ and $n=\pm 2r$ (k and r are positive integers). From (I-19), we find the diffraction maxima directions:

$$s_{2k}=kz_0^{-1}. \tag{7}$$

The superstructure factor is defined by (I-25b) and (I-25c) or by (I-A11b). At $\mathbf{hb}>0$, the diffraction maxima for $l>0$ and $l<0$ are due to the reflections from the blocks $y>0$ and $y<0$, respectively. The dependences of $|M_{2k,2r}|$ *versus* Y are presented in Fig. 2.

For the diffraction maximum $l=2$ we have [see (I-B6)]

$$M_{2,2r}=rq^{(r-1)/2}(1-q). \tag{8}$$

The superstructure factor of the principal maximum is

$$M_{2,2}=1-q. \tag{9}$$

The satellite superstructure factor has a maximum

$$|M_{2,2r}|_{max}=[2r/(r+1)][(r-1)/(r+1)]^{(r-1)/2} \tag{10}$$

at

$$q_1=(r-1)/(r+1) \tag{11}$$

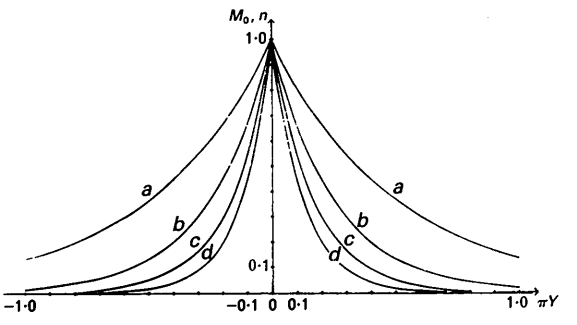

Fig. 1. Function $|M_{0,n}(Y)|$. (a) $n=2$; (b) $n=4$; (c) $n=6$; (d) $n=8$.

or at

$$Y_1 = 2\pi^{-1} \ln [(r+1)/(r-1)]. \quad (12)$$

The value of $|M_{2,2r}|_{max}$ is nearly independent of n and is approximately equal to

$$|M_{2,2r}|_{max} \simeq 2e^{-1} \simeq 0{\cdot}74. \quad (13)$$

With increasing r the location of the maximum shifts towards the boundary.

(3) *Odd l*

Let $l = 2k-1$ (k is a positive integer). From (I-19) we find the diffraction maxima directions:

$$s_{2k-1} = (2k-1)/2z_0. \quad (14)$$

The superstructure factor is defined by (I-25*d*) and (I-25*e*) or (I-*A*13*b*) and (I-*A*14*b*).

As seen from (2*c*), at odd l the reflection from the boundary between blocks takes place for all the diffraction maxima of an odd l, contrary to the case of an even l when only the satellite $l = 0$ is reflected from the boundary. This is because at odd n the phase shift is π times an odd number Another difference is that the diffraction maxima of an odd order are reflected from both blocks, but the reflection is asymmetric with respect to the boundary (Figs. 3 and 4). At **hb** > 0 and $l > 0$ the curve $|M_{l,n}(Y)|$ has a faint 'tail' in the block $y < 0$.

3. Kinematic profiles

Under the condition of

$$D \ll \Lambda_{l,n} = \bar{\Lambda}/|M_{l,n}|, \quad (15)$$

where D is the crystal thickness, $\Lambda_{l,n}$ and $\bar{\Lambda}$ are the SL and crystal extinction lengths, respectively, and using (I-11) for the lth-order diffraction maximum intensity we obtain the kinematic formula

$$R^{kin}_{l,n} = (\pi D/\bar{\Lambda})^2 |M_{l,n}|^2. \quad (16)$$

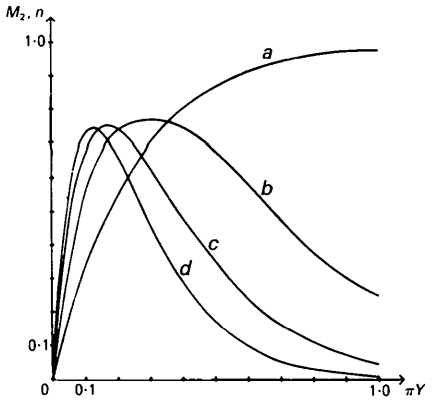

Fig. 2. Function $|M_{2,n}(Y)|$. (*a*) $n = 2$; (*b*) $n = 4$; (*c*) $n = 6$; (*d*) $n = 8$.

The forms of the kinematic image profiles are qualitatively the same as that of the $|M_{l,n}(Y)|$ (see Fig. 4 of paper I).

At $l = 0$ there is only one fringe with maximum intensity on the boundary, the intensity profile being symmetric with respect to the boundary. The fringe width is determined by (6):

$$\Delta Y = (\pi|n|)^{-1} \ln 2 \quad (17)$$

and decreases with increasing $|n|$.

From (I-16) and (I-1) we obtain

$$\Delta y = (\pi|n|)^{-1} z_0 \ln 2 = (\pi h \Delta\theta)^{-1} \ln 2, \quad (18)$$

i.e. the fringe width is less than the effective thickness of the dislocation wall. It means that the spatial harmonic $l = 0$ propagates through a narrow 'channel' along the boundary. With the increasing disorientation of the blocks the 'channel' width contracts.

At $l = 1$ and $l = 2$ there is a single fringe, shifted from the boundary. With increasing n the fringe width decreases and the fringe center shifts towards the boundary, while the intensity is almost the same.* For these spatial harmonics the diffraction channel is away from the boundary. At $l \geq 3$ the image consists of a number of parallel fringes, the number of which is determined by the number of $|M_{l,n}|$ maxima (4).

* In fact the intensity decreases since the crystal structure factor F_h decreases with the increasing reflection order. The question here is about the relative intensity.

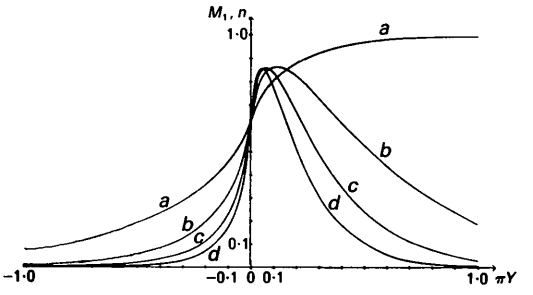

Fig. 3. Function $|M_{1,n}(Y)|$. (*a*) $n = 1$; (*b*) $n = 3$; (*c*) $n = 5$.

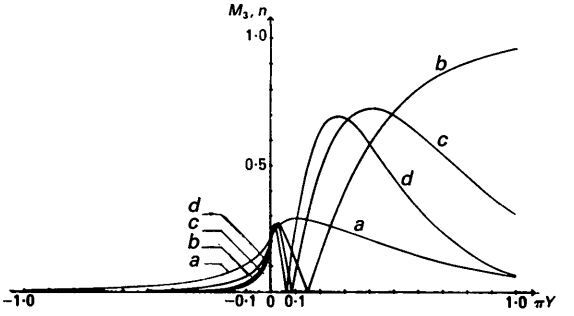

Fig. 4. Function $|M_{3,n}(Y)|$. (*a*) $n = 1$; (*b*) $n = 3$; (*c*) $n = 5$.

The further a fringe is from the boundary, the wider and more intense it is, with a relatively extended tail. Far from the boundary the fringe separation increases. For a given spatial harmonic l the fringes are from only one side of the boundary. At odd l the image has a short tail on the other side of the boundary. At $l = n$ (the principal maximum of one of the blocks) the image has the form of a wide fringe at one side of the boundary with a number of parallel narrow fringes towards the boundary.

4. Dynamical profiles

If the condition (15) does not hold then the wave multifold reflections cannot be neglected. In this case the reflection intensity is defined by (I-11).

At $s = s_l$, from (I-11) we have

$$R_{l,n}^{\mathrm{dyn}} = \sin^2(\pi A|M_{l,n}|), \tag{19}$$

where

$$A = D/\bar{\Lambda}. \tag{20}$$

In Figs. 5-7 the plots of $R_{l,n}^{\mathrm{dyn}}(Y)$ for several values of l and n at $A = 2$ and 2·5 are given. The comparison of the kinematic and dynamical profiles indicates that they differ significantly. For the dynamical profiles, the number of fringes and their widths depend on A. In the kinematic profiles, the intensity oscillations are due to the type of strain distribution present in the dislocation SL cell. On the dynamical profiles the intensity oscillations are associated with the *Pendellösung* oscillations analogous to those visible in ideal crystals.

For the harmonics with even $l \neq 0$ the boundary image is one sided as in the kinematic case. For the harmonics with odd l, the image arises on both sides from the boundary (Fig. 7). Because of the *Pendellösung* effect the wide fringe of the principal maximum is either absent (A being an integer) or is a maximum of intensity (A being a semi-integer).

As we have already noted, the spatial harmonic $l = 0$ at small depths has a sharp peak on the boun-

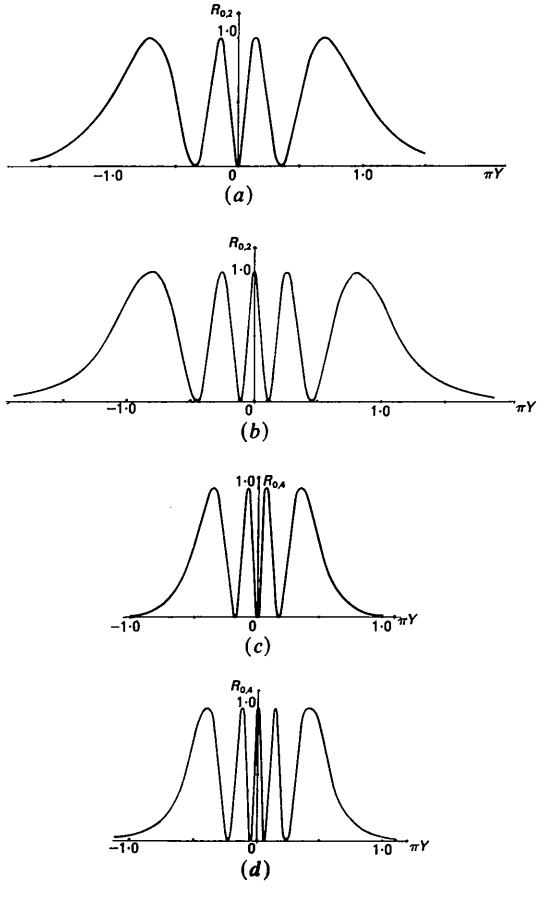

Fig. 5. Dynamical profiles for $l = 0$. (*a*) $n = 2$, $A = 2$; (*b*) $n = 2$, $A = 2{\cdot}5$; (*c*) $n = 4$, $A = 2$; (*d*) $n = 4$, $A = 2{\cdot}5$.

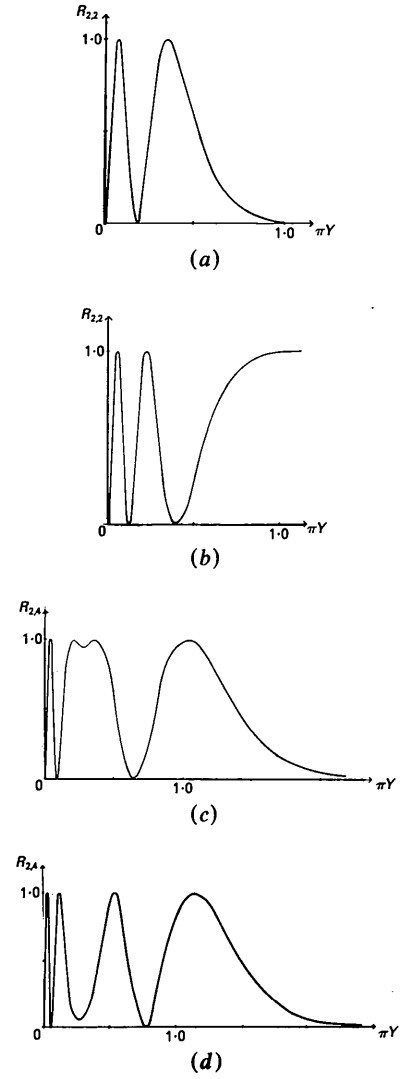

Fig. 6. Dynamical profiles for $l = 2$. (*a*) $n = 2$, $A = 2$; (*b*) $n = 2$, $A = 2{\cdot}5$; (*c*) $n = 4$, $A = 2$; (*d*) $n = 4$, $A = 2{\cdot}5$.

dary. At depths when the dynamic scattering becomes essential this peak splits into a number of peaks arranged symmetrically with respect to the boundary (Fig. 5).

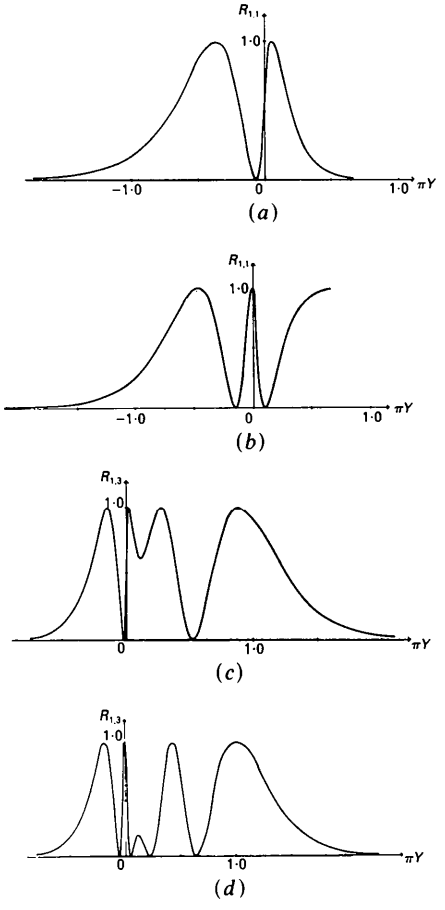

Fig. 7. Dynamical profiles for $l=1$. (*a*) $n=1$, $A=2$; (*b*) $n=1$, $A=2{\cdot}5$; (*c*) $n=3$, $A=2$; (*d*) $n=3$, $A=2{\cdot}5$.

5. Concluding remarks

The basic rules obtained in considering X-ray diffraction by a crystal with a twist boundary perpendicular to the crystal surface make it possible to investigate the structure of the boundary-side layer of bicrystals. The direct-image method (Amelinckx & Dekeyser, 1959) and the diffraction-image method suggested in this work complement each other, but the latter makes it possible to perform a more detailed study of the boundary-side layer structure. In the present work we did not take into account wave-field absorption and the incident-beam divergence. Absorption is important for thick crystals and will cause softening of the *Pendellösung* fringe contrast due to the anomalous absorption effect. The incident beam divergence, essential in the X-ray case, leads to the consideration of an incident spherical wave. In this case the form and the arrangement of the *Pendellösung* fringes will be different.

It can be shown that if there is a deviation from the periodicity in SL, the situation is analogous to the thermal diffuse scattering of X-rays by crystals and can be described by an analog of the Debye-Waller factor.

References

AMELINCKX, S. & DEKEYSER, W. (1959). *Solid State Phys.* **8**, 325.
BATEMAN, H. & ERDELYI, A. (1953). *Higher Transcendental Functions.* Vol. I. New York: McGraw-Hill.
RUNCKEL, H. J. (1971). *Math. Ann.* **191**, 53–58.
VARDANYAN, D. M. & MANOUKYAN, H. M. (1982). *Phys. Status Solidi A*, **69**, 475–482.
VARDANYAN, D. M. & MANOUKYAN, H. M. (1985). Proc. Conf. on the Problems of X-ray Diagnostics of Crystal Imperfection, Yerevan, Armenia, USSR.
VARDANYAN, D. M. & PETROSYAN, H. M. (1987). *Acta Cryst.* A**43**, 316–321.

Acta Cryst. (1987). A**43**, 326–337

A New Method of Deriving and Cataloguing Simple and Multiple Antisymmetry G_3^l Space Groups

BY S. V. JABLAN

The Mathematical Institute, Knez Mihajlova 35, Belgrade, Yugoslavia

(*Received* 24 *June* 1986; *accepted* 30 *October* 1986)

Abstract

Antisymmetric characteristics of 230 (Fedorov) G_3 space groups are constructed. By application of a partial cataloguing method based on a newly defined term of antisymmetric characteristic type, a partial catalogue of simple and multiple antisymmetry M^m-type space groups and numbers of these groups are obtained.

The G_3^l space groups of simple and multiple antisymmetry, derived from the 230 Fedorov G_3 space groups,

0108-7673/87/030326-12$01.50